

High resolution geochemical and grain-size analysis of the AD 1755 tsunami deposit: Insights into the inland extent and inundation phases

Sandra Moreira^{a,b,*}, Pedro J.M. Costa^{a,**}, César Andrade^a, Cristina Ponte Lira^a, Maria Conceição Freitas^a, Maria Alexandra Oliveira^a, Gert-Jan Reichart^{c,d}

^a Instituto Dom Luiz and Departamento de Geologia, Faculdade de Ciências, Universidade de Lisboa, Edifício C6, Campo Grande, 1749-016 Lisboa, Portugal

^b Instituto Hidrográfico - Marinha, Rua das Trinas, 49, 1249-093 Lisboa, Portugal

^c NIOZ Royal Netherlands Institute for Sea Research, Texel, The Netherlands

^d Department of Earth Sciences, Geosciences Faculty, Utrecht University, Utrecht, The Netherlands

ARTICLE INFO

Keywords:

Geochemistry
Grain-size image analysis
Palaeotsunami
Inundation
Backwash
Portugal
AD 1755 tsunami

ABSTRACT

In the study of palaeotsunamis it is crucial to decipher the sedimentological record, to derive intensity of past events and to infer different inundation phases. To achieve this goal, it is important to apply high-resolution techniques that allow magnifying intra-deposit details (at a sub-centimetric scale) that otherwise would not be perceived; consequently, valuable information could be overlooked.

In this work, we applied successfully high-resolution geochemical and grain-size analyses – XRF core-scanning and image analysis, respectively – to the AD 1755 tsunami deposit. This quartz sand enriched in bioclast deposit (exhibiting high Si/Al and Ca/Ti) was recognized in the coastal stratigraphic sequence of Salgados lagoon due to its contrasting composition when compared with the under and overlying mud layers with scarce bioclasts (exhibiting low Si/Al and Ca/Ti). In the absence of textural evidence, the identification of peaking concentrations of Cl, S and Br (all major constituents of sea salt) in a continuous muddy sequence allowed slightly extending farther inland the limit of inundation. In addition, grain-size analysis data attested the fining inland of the deposit. Furthermore, despite the macroscopic massive structure of the tsunami deposit, throughout the lagoon, grain-size results revealed more complexity and allowed inferring up to four depositional sequences directly associated with the AD 1755 tsunami inundation.

1. Introduction

Scientific literature related to tsunami deposits have been published after the late 1980s (see Atwater, 1987; Dawson et al., 1988; Goff et al., 2012). In particular, a large number of publications followed the 26th December 2004 Indian Ocean and the 11th March 2011 Japanese tsunamis, focusing on sedimentological, geomorphological and biological imprints (e.g. Paris et al., 2010; Etienne et al., 2011; Chagué-Goff et al., 2011; Jagodziński et al., 2012; Tappin et al., 2012; Szczuciński, 2012; Goto et al., 2014; Toyofuku et al., 2014). Innovative techniques (such as computerized tomography) have been applied to extract hydrodynamic information from tsunami deposits (Falvard and Paris, 2016). Despite this recent progress, researchers still rely mainly on using sedimentological, stratigraphical and micropalaeontological proxies to identify sediment layers deposited by both historical and pre-historical tsunamis. Based on the existing literature, it is clear that a single technique

or a single sediment characteristic by itself does not suffice to, unequivocally, associate a particular deposit with a tsunami-related origin.

Recently, the use of (semi)quantitative geochemical analysis rapidly expanded with the application of core-scanning techniques to tsunami deposits [see Chagué-Goff et al. (2017) for details]. As suggested by Chagué-Goff et al. (2015), geochemical signatures might provide crucial data when other lines of evidence are not available or have not been preserved. Still, these authors also recommend that geochemistry should be used in conjunction with other environmental or source-sensitive proxies.

Recent contributions of geochemical analyses in contemporaneous tsunami deposits focused on the definition of the maximum inundation limit, because the landward distance at which tsunami sediments are deposited in the coastal zone is, in general, smaller than the horizontal penetration reached by the tsunami inundation (e.g. Morton et al.,

* Correspondence to: S. Moreira, Instituto Dom Luiz and Departamento de Geologia, Faculdade de Ciências, Universidade de Lisboa, Edifício C6, Campo Grande, 1749-016 Lisboa, Portugal.

** Corresponding author.

E-mail addresses: sandra.moreira@hidrografico.pt (S. Moreira), ppcosta@fc.ul.pt (P.J.M. Costa), candrade@fc.ul.pt (C. Andrade).

2011; Abe et al., 2012; Chagué-Goff et al., 2012a). This can be of great relevance for the reevaluation of inundation limits of some historical and all pre-historical tsunamis, which were previously underestimated (e.g. the CE 869 Jogan tsunami — Goto et al., 2011; Sugawara et al., 2012; Namegaya and Satake, 2014).

Tsunami deposits present quite a wide range of sedimentary characteristics, such as grain-size distribution and sedimentary structures, which are influenced by local bathymetry and topography, sources of sediment and transport processes (Sugawara et al., 2008). Analyzing the overall sediment texture is the main and most commonly applied proxy to identify tsunami deposits. Grain-size parameters contribute to the description of tsunami deposits and are used to infer the origin of the displaced sediment and to identify the hydrodynamic conditions responsible for tsunami deposition (Chagué-Goff et al., 2011). Tsunami deposits are often recognized by a distinct fining-upward depositional sequence (Benson et al., 1997; Bondevik et al., 1997; Gelfenbaum and Jaffe, 2003), which is mainly due to free re-settling of particles related to a decrease of the turbulence of the flow after the tsunami has retreated. However, also non-graded (massive), coarsening-upwards or multiple graded sand sheets have also been associated with tsunami deposition (Benson et al., 1997; Bondevik et al., 1997; Gelfenbaum and Jaffe, 2003; Szczuciński, 2012).

Several methodologies for grain-size analysis (e.g. sieving, laser diffraction and settling velocities) have been used. However, despite recent developments in the use of digital image analysis to obtain grain-size data (Lira, 2011; Buscombe, 2013; Lira, 2015) and to the best of our knowledge, high resolution (*i.e.* at millimetric scale) data have not yet been exploited as an additional tool to better understand tsunami sedimentary dynamics.

Despite recent progresses in the recognition of the AD 1755 tsunami deposit in southern Portugal (e.g. Costa et al., 2012a), and in the establishment of its sediment source (Costa et al., 2012b; Costa et al., 2015) and run-up height (Costa et al., 2016), inundation phases were not identified based on its geological signatures. This study aims to resolve this gap, applying high-resolution geochemical and textural data, complemented with heavy mineral analysis.

2. Study area

2.1. The AD 1755 event

Despite their low frequency of occurrence, tsunamis are known to have impacted the Iberian Peninsula coasts multiple times. The largest tsunami that affected the Atlantic coasts of Europe in historical times was the well-known AD 1755 tsunami, which followed the so-called Lisbon earthquake. The AD 1755 tsunami source area has been challenged in recent years (e.g. Zitellini et al., 2001; Baptista et al., 2003; Gutscher et al., 2006; Grandin et al., 2007; Barkan et al., 2009), with no consensus having been reached so far over triggering mechanism and precise location of the source. Shortly after the earthquake, the tsunami impacted the coasts of Iberia and Morocco, reaching cape São Vicente (Fig. 1A), on the Algarve coast of Portugal, after 15 min, Huelva after 45 min and Cadiz after 78 min. Lisbon, located inside an estuary, was hit 90 min after the earthquake (Baptista et al., 1998) (Fig. 1A). The tsunami effects were felt also across the Atlantic up to the Gulf of Mexico (Atwater et al., 2012). Detailed documentary records of the AD 1755 event and impacts have been summarized by several authors (e.g. Lopes, 1841; Sousa, 1919; Oliveira, 2005). The first three tsunami waves were particularly destructive along the west and south coasts of Portugal (Oliveira, 2005).

2.2. The Algarve coast and Salgados lagoon

The Salgados lowland is located in the bay between Armação de Pêra and Galé (Fig. 1B). This coastal ribbon consists of a 6 km-long intermediate-reflective sand beach, backed by a continuous 3 to 17 m-

high vegetated dune ridge (Fig. 1C). The dune sand covers resistant Pleistocene-Holocene aeolianite and beachrock (Moura et al., 2007). The beach-dune system continuity at the Salgados inlet is ensured by a welded sand barrier. Inputs of marine water are caused by wave overwash of the barrier or occur when the maximum lagoonal water level is reached and the barrier is breached, allowing the outflow of the water and the entrance of marine water through a tidal inlet. The Salgados lagoon was ca. 1.5 km² wide, but about half of this surface has been reclaimed and landfilled for a golf course in 1988. The remnant surface is a flat-floored depression 1.1 to 1.7 m above mean-sea level (*msl*), collecting water and muddy sediment from the adjacent catchment.

3. Sampling

Lagoa dos Salgados was temporarily drained by the Portuguese Environmental Agency (APA) in October 2013, creating an ideal opportunity to conduct detailed Holocene stratigraphic studies in the lagoonal area, which is, under normal circumstances, permanently flooded. Five trenches (Fig. 1C) were excavated along a North-South orientation, with dimensions of approximately 1 m (depth) × 3 m (width) × 5 to 10 m (length). Six box-cores (approximately 30 × 12 × 10 cm) were retrieved from the trench walls for subsequent textural and geochemical analyses. One box-core was collected from each of the four southernmost trenches (SG_T1 to SG_T4). In the northernmost trench (SG_T5) the tsunami deposit reduced to an extremely thin, discontinuous and irregular sandy lamina, therefore this trench was extended northward far beyond the point where the tsunami sand disappeared within the mud (Fig. 2A). Here, two box-cores were collected from the same wall and < 10 m apart from each other: SG_T5#2, showing tsunami sand sandwiched in lagoonal mud, and SG_T5#1, collected at an analogous depth but with no macroscopic evidenced of a tsunami deposit (Fig. 2B).

4. Analytical methods

Geochemical analyses were performed using an Avaatech X-Ray Fluorescence (XRF) core-scanner at the Royal Netherlands Institute for Sea Research (NIOZ). This is a non-destructive methodology where bulk-sediment chemistry measurements are performed directly on the sediment surface. The box-core sediment surface was cleaned, leveled and covered with a thin (4 µm) Ultralene film to avoid contamination of the measurement prism of the scanner and desiccation of the sediment, following Tjallingii et al. (2007). The optical system of the Avaatech core scanner is He-flushed (Rothwell and Croudace, 2015) and is in contact with the covering film during measurement to allow accurate measurement of light elements. The X-ray beam (3 mm long × 12 mm wide) sequentially irradiated an area of 36 mm², using a step-size of 3 mm. Two ionization energies were used (10 kV for 10 s and 30 kV for 20 s). Semi-quantitative data for a total of 20 elements (10 kV — Al, Si, S, Cl, K, Ca, Ti, Cr, Mn; 30 kV — Fe, Ni, Cu, Zn, Ga, Br, Rb, Sr, Y, Zr and Pb) were obtained, but only those used in the context of this study are presented here. Raw count data were processed using the manufacturers' software (Avaatech), providing semi-quantitative elemental data. The analytical precision of XRF was assessed by three-fold measurements repeated every 6 cm, in a total of 30 different positions, corresponding to the proportional deviation (in %) from the arithmetic mean of those measurements (Westerhold, 2003; Tjallingii, 2006). In what concerns the 10 kV measurements, abundant elements like Si and Ca were reproduced within a precision of ± 2%. For Al, S, Cl, K and Ti the deviation became larger than ± 4.5%, when element intensities were less than ~8000 counts (with a few exceptions, such as for Cl). The 30 kV measurements that retrieved values for Br and Zr displayed a scatter of ± 18%, independently of the range of elemental intensities. Factors influencing the measurements in this type of analysis are discussed in Tjallingii et al. (2007) and Löwemark et al. (2011). Further

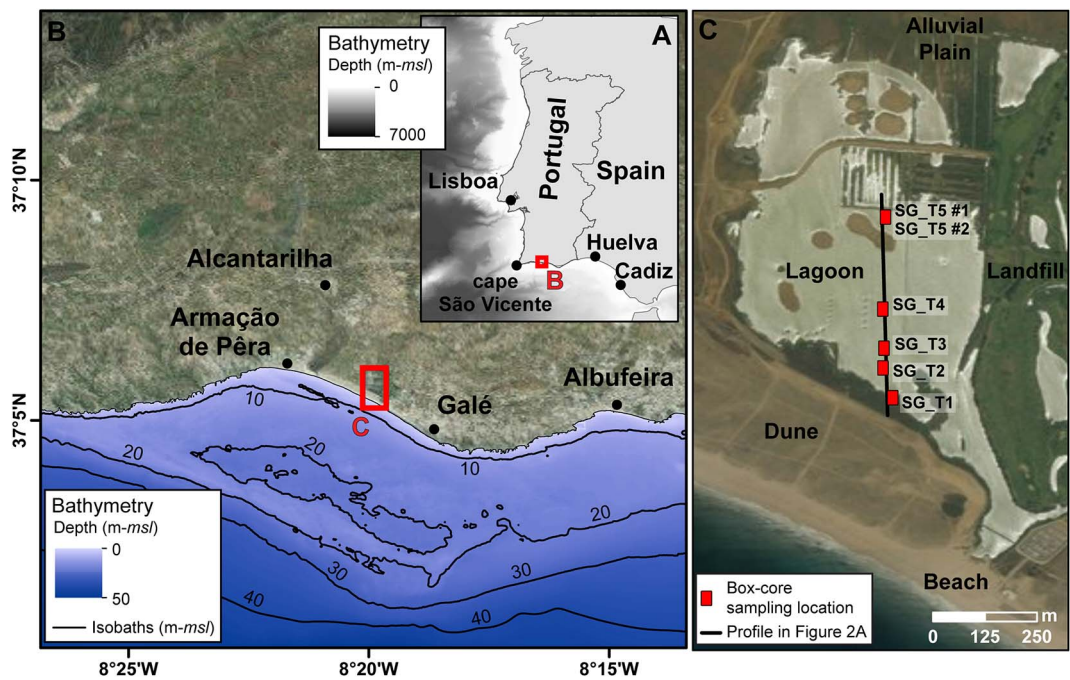


Fig. 1. A and B) Location of study site in the south coast of Portugal. C. Location of the five trenches in the Salgados lagoonal basin. Satellite image sourced by Esri, DigitalGlobe, GeoEye, Earthstar Geographics, CNES/Airbus DS, USDA, USGS, AeroGRID, IGN, and the GIS User Community. Regional bathymetry built from data of the Hydrographic Institute of the Portuguese Navy and local bathymetry provided by Joaquim Luis from Algarve University.

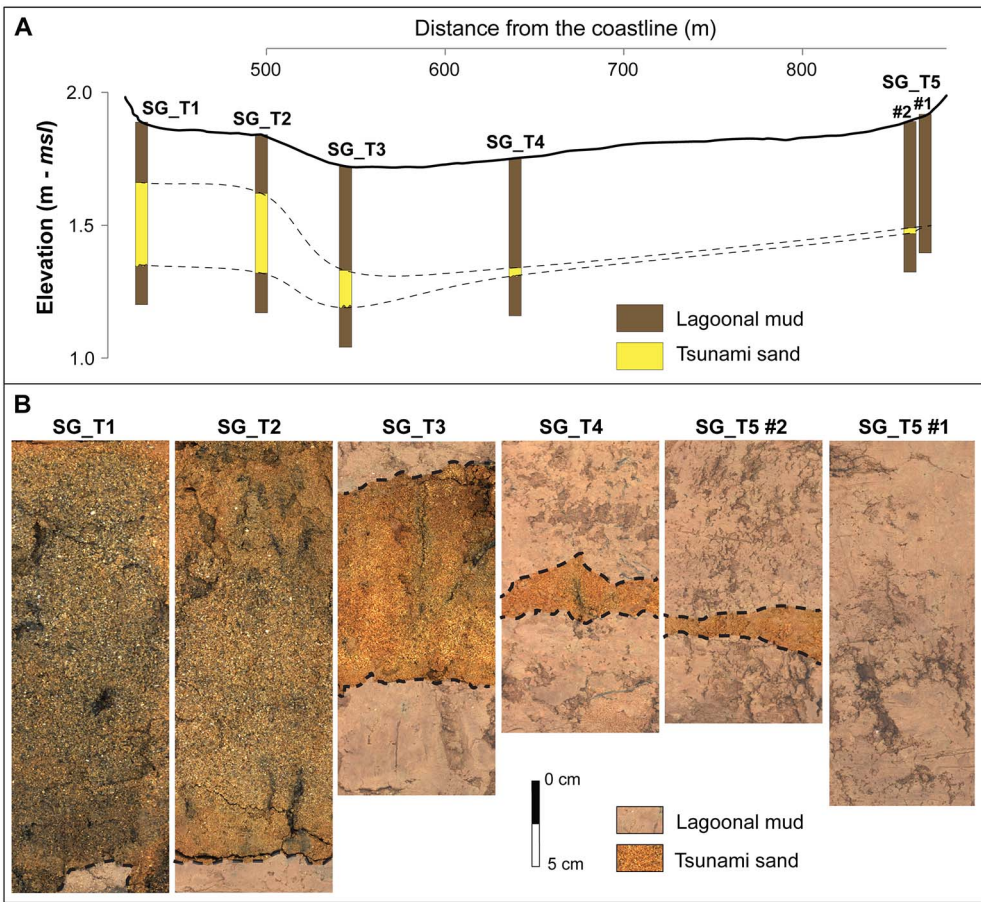
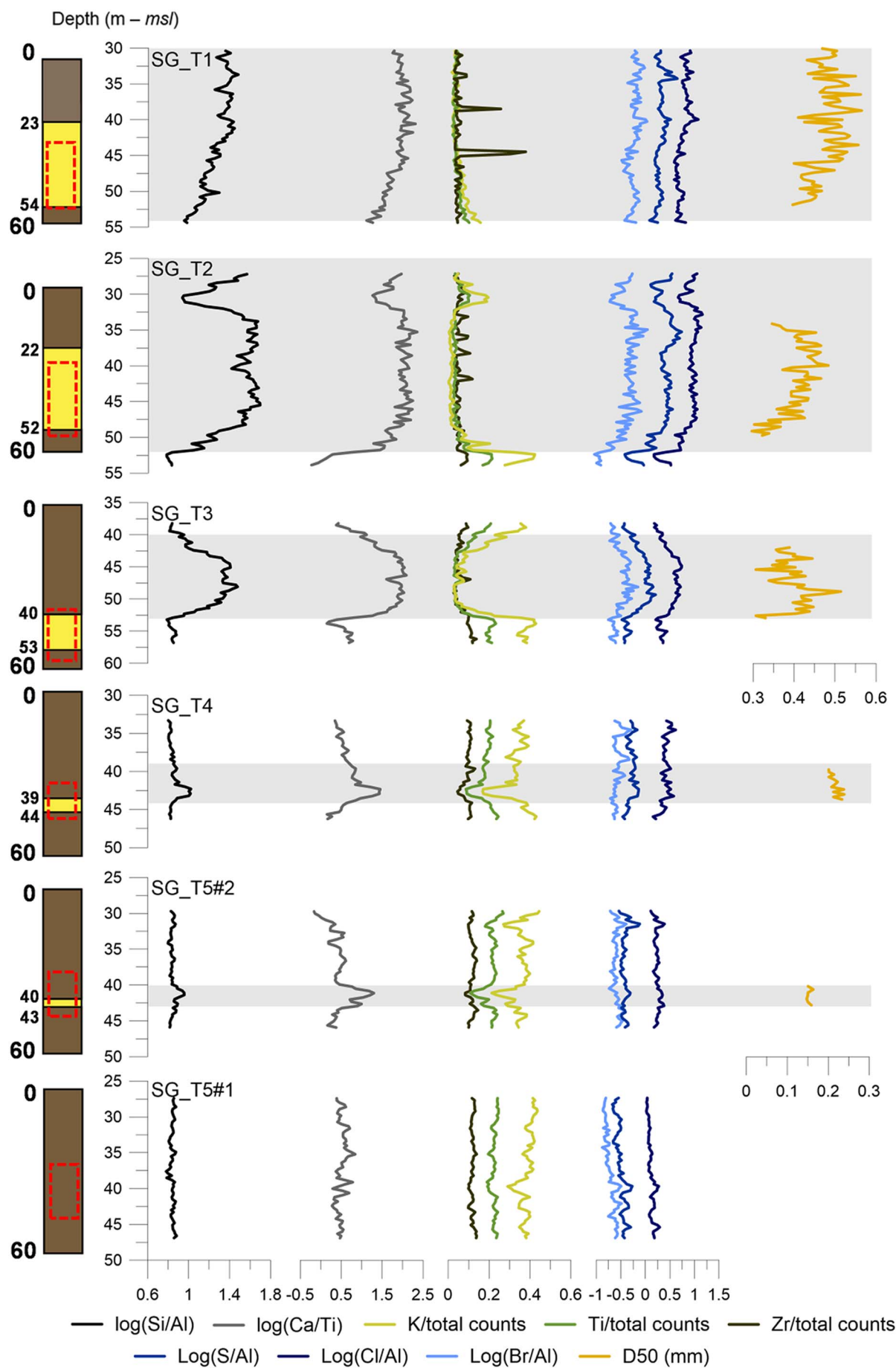


Fig. 2. A. Cross-shore topographic profile containing a representation of the tsunami deposit within lagoonal mud (*msl* — mean sea level). B. High resolution photographs of the sampled box-cores, with delimitation of the sandy tsunami deposit (black dash line).



(caption on next page)

Fig. 3. Identification of box-core sampling depths in each trench wall and vertical variation of Si/Al, Ca/Ti, K/total counts, Ti/total counts, Zr/total counts, Cl/Al, Br/Al and S/Ti values in the sampled sediments of Salgados lagoon.

information on method used and calibration procedures followed are described in Richter et al. (2006).

The chemical composition of the sediment is reported in counts per second, this value being proportional to the concentration of each element in the bulk sediment. For Ti, Fe and Zr, results are given as ratios between elemental counts and total counts obtained. Elemental data for Si, Ca, Cl, S and Br have been Al- or Ti-normalized in order to mitigate the effects of textural variability, as discussed, for example, in Brumsack (2006). According to Weltje and Tjallingii (2008) results are presented as log-ratios.

In addition to geochemical measurements, high-resolution digital images (Fig. 2B) were simultaneously obtained for each box-core using a JAI 4 CCD Line Scan Camera coupled with the core-scanner. Grain-size analysis of the sand fraction was conducted with image analysis (IA) techniques (Lira and Pina, 2007), using an automated methodology described in Pina et al. (2011), with adaptations presented in Lira (2011, 2015). This IA method allows assessing the full grain-size distribution of particles larger than 0.063 mm, using the correlation between image intensity values and particle area. The particle area is then approximated to a sphere of equivalent diameter. A drawback of this method is that grains smaller than 0.063 mm cannot be perceived as individual objects due to image resolution constraints, thus results for finer fraction cannot be computed. Nevertheless, this methodology allowed mimicking the geochemical analytical resolution, and median grain-size (D50) was computed using a window of 3×12 mm across each box-core.

A total of 17 discrete samples (~ 1 cm thick) from SG_T1, T2 and T4 were chosen in order to identify heavy minerals (HM) within the tsunami deposit. Sample intervals were based on Zr peaks detected using the XRF analyses, to investigate possible correlations with percentages of zircon, which is the main mineral carrier of this element. Samples were washed in tap water and subsequently sieved at 0.5Φ intervals. Next, the $1 < \Phi \leq 3$ ($125 \leq \mu\text{m} < 500$) fractions of the sieved sand were gathered and HM separated using bromoform. The HM fractions were further split and mounted on glass slides with Entellan resin. About 300 HM particles per slide were individually identified and counted under an Olympus BX40 petrographic microscope. The grain-size data from the sieved samples were used to validate the image-based grain-size data, and the respective statistical parameters were derived using the graphic method (Folk & Ward, 1957).

5. Results

5.1. Mid-Late Holocene lagoonal lithostratigraphy and AD 1755 tsunami imprint

The sedimentary infill of Salgados lagoon consists of muddy and sandy sediment that accumulated during the Mid-Late Holocene (ca. 5900 yrs BP to present — Costa et al., 2012a). Within the topmost mud-dominated unit (which is 0.70 to 1.90 m thick), a single and macroscopically massive, laterally continuous, sand layer was found, at app. 0.4 m below surface (bs) (Costa et al., 2012a). This layer has been associated with the AD 1755 tsunami and consists essentially of medium to fine quartz sand, with marine shell fragments and muddy rip-up clasts (Costa et al., 2012a). The sandy tsunami deposit contrasts markedly with the underlying and overlying muddy units of lagoonal facies, and is separated from the basal sediments by an unconformity. The tsunami deposit is widely distributed in the lagoonal basin and shows a decreasing thickness inland (from 0.80 m to a few mm), until its landward limit, ca. 850 m from the present-day coastline. The elevation of the basal contact of the tsunami unit rises gradually inland from about + 0.05 to + 1.28 m msl (Costa et al., 2012a).

Dating results (^{14}C , ^{210}Pb and ^{137}Cs) allowed the extrapolation of an age of deposition compatible with the AD 1755 Lisbon earthquake and tsunami (Costa et al., 2012a). Microtextural, grain-size and heavy minerals analysis (Costa et al., 2012a, 2015) suggest that the primary sources of the event deposit were the adjacent dune and beach sediments added by small contribution of mud eroded from the lagoonal bottom.

Lithostratigraphy of the trench sections are summarized in Fig. 2A and agree with previous descriptions for the topmost meter of the lagoonal sedimentary sequence (Costa et al., 2012a).

The sand of the AD 1755 tsunami deposit presents similar thickness (31 and 30 cm, respectively) in both southernmost trenches (SG_T1 and T2) and is thinner in trenches located further landward (Fig. 2A). The sedimentary sequence exposed in trenches SG_T1 and T2 was only partially sampled (Fig. 3) due to limitations with box-coring length and packing, which made it difficult to fully preserve the topmost part of the tsunami deposit. Here, the basal contact is sharp/erosive and is located at 54 and 52 cm bs (equivalent to 1.35 and 1.32 m msl), respectively (Fig. 2).

In SG_T3 the lower limit of the tsunami sand is well defined at 53 cm bs (1.19 m msl), while the upper limit is observed at around ~ 40 cm bs (1.32 m msl), resulting in a total thickness of ~ 13 cm (Fig. 2).

In SG_T1, T2 and T3 it was possible to identify macroscopically, at the base of the tsunami deposit layer, a section (with thickness of app. 3, 2 and 1 cm respectively) composed of finer sand (Fig. 2B).

In trench SG_T4 the tsunami deposit is thin and severely bioturbated, showing uneven upper and lower limits, which are roughly located at 39 and 44 cm bs (1.36–1.31 m msl) (Fig. 2). However, its upper limit is less well-defined in comparison with the basal one.

In trench SG_T5, the tsunami deposit was rather discontinuous, with irregular upper and lower boundaries, and with its thickness varying laterally along the trench wall (Fig. 2). In general, the layer represented by box-core SG_T5_#2 could be traced between 40 and 42/43 cm bs (1.46–1.47 to 1.49 m msl). In box-core SG_T5_#1 no macroscopical differences were noticeable in texture, hence no tsunami deposit was visible (Fig. 2B).

5.2. Geochemistry

The most evident results based on the semi-quantitative geochemical analysis are the changes in downcore profiles of Si/Al, Ca/Ti, K-, Ti- and Zr/total counts (Fig. 3), which record the overall composition of the sediment. Broadly, Si/Al and Ca/Ti log-ratios translate changes in texture and carbonate content of the sediment, showing similar vertical variation patterns in all box-cores. The K-, Ti- and Zr/total counts ratios exhibit similar behavior but show opposite changes relatively to the former ratios, because these elements usually occur in higher relative abundances in muddy sediments. All these ratios allow differentiation of the sandy layer associated with the AD 1755 tsunami event from the muddy lagoonal sediment.

In box-cores SG_T1 to T5_#2 (Fig. 3), distinctly higher values of Si/Al and Ca/Ti correspond to sandy sediments with bioclasts, which are sandwiched within mud with lower values of both ratios. Hence, major compositional breaks coincide with the limits of the tsunami deposit, as defined in the field. However, changes tend to be more evident at the lower limit of the event-layer, corresponding to the abrupt change between the lower mud and the tsunami deposit, whereas the upper contact is subtler, with a gradual upward decrease of both ratios. Despite the fact that in the sandy deposit the contents of K, Ti and Zr are lower in comparison with the lagoonal muds, a number of peaks in Zr were detected in the sandy deposit sampled in SG_T1 to SG_T4 (Fig. 3). In SG_T1 three peaks are clearly identified at 44.5, 38.5 and 34 cm bs,

Table 1
Statistical parameters of the median grain-size along the tsunami sand by image analysis (IA).

Box-core	Minimum–maximum (range) (μm)	Average \pm standard deviation (μm)	CV ^a (%)
SG_T1	395–564 (169)	476 \pm 41	8.6
SG_T2	295–482 (187)	403 \pm 44	10.8
SG_T3	306–514 (208)	398 \pm 46	11.5
SG_T4	201–239 (38)	217 \pm 13	6.2
SG_T5#2	147–163 (16)	153 \pm 5	3.5

$$^a \text{CV (\%)} = \frac{\text{Standard deviation}}{\text{Average}} \times 100.$$

with maximum values decreasing towards the top of the layer. The general pattern of Zr/total counts along SG_T2 is interrupted by distinctive increases of this ratio at 42, 38, 36, 33 and 30 cm *bs*. In SG_T3 a well-defined peak of Zr, K and Ti, occurs at 47 cm *bs*. A single peak of Zr is observed in SG_T4, at 39.5–40 cm *bs*.

In box-core SG_T5#1, without macroscopic textural differences being observed in the field, the Si/Al values (and also Ti- and Zr/total counts) are roughly uniform (Fig. 3).

Major constituents of sea salt such as Cl, S and Br, display similar behavior, despite that the highest Al-normalized values of these elements are observed at different depths (Fig. 3). Moreover, the downcore variation of these ratios also change concomitantly with Si/Al and Ca/Ti. However, the maxima of these elements do not occur exclusively in the sandy tsunami deposit, as observed in box-cores SG_T4 and T5#2. For box-core SG_T5#1, after Al-normalization, all salinity indicators show higher ratios below *ca.* 37 cm *bs*. Still, a maximum value is observed at *ca.* 39 cm *bs* in the downcore records of Cl-, S- and Br/Al log-ratios. In SG_T5#2, at that specific depth, the sandy tsunami deposit is visually identified.

5.3. Grain-size

As observed in Fig. 3, the median grain-size (D50) of the tsunami deposit, as computed by IA, decreases inland. Grain-size results obtained with IA, as well through standard sieving analysis, are summarized in Table 1 showing that both methods provide similar results, which are translated in a correlation coefficient (*R*; Andrade et al., 2003) of 0.84 (Fig. 4).

The tsunami deposit is composed by medium to coarse sand in

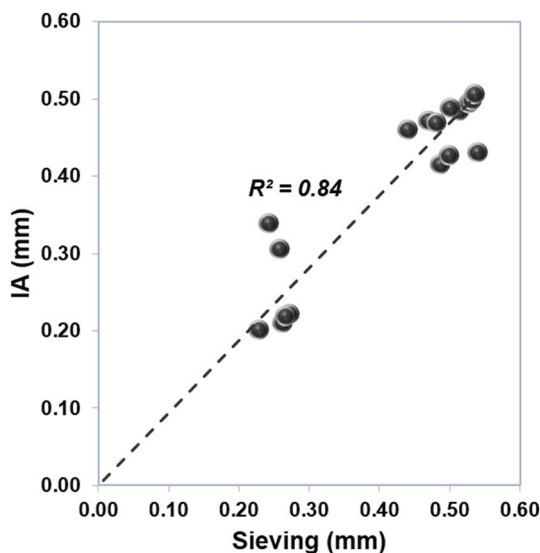


Fig. 4. Comparison of median grain-size (D50) values obtained from sieving and image analysis (IA) of tsunami sand from the box-cores SG_T1, SG_T2 and SG_T4. The linear best fit line was forced to cross the axes origin.

SG_T1, medium sand in SG_T2 and T3 and fine sand in SG_T4 and T5#2 (Fig. 3, Table 1). Both the vertical profiles of D50 in each box-core and the corresponding curve of moving average (three consecutive measurements) (Figs. 5 and 6) indicate that the tsunami layer incorporates different sediment packages. Still, within each individual box-core, the median grain-size of the tsunami sandy layer shows relatively low variability, as indicated by a coefficient of variation between 3.5 and 11.5% (Table 1).

In the case of SG_T1 four major packages are apparent (Fig. 5): a) a massive or coarsening-upward (*i.e.* inverse graded) basal sequence up to 46 cm *bs* (~8 cm thick), with grain-size varying between 395 and 497 μm , and finer compared to the overlying sand; b) a fining-upward (*i.e.* normal graded) sequence from 46 to 39.5 cm *bs* (6.5 cm thick), with median grain-size varying between 409 and 556 μm ; c) a fining-upward sequence from 39.5 to 31.5 cm *bs* (8 cm thick), with median grain-size ranging from 430 to 564 μm ; and d) the likely start of a

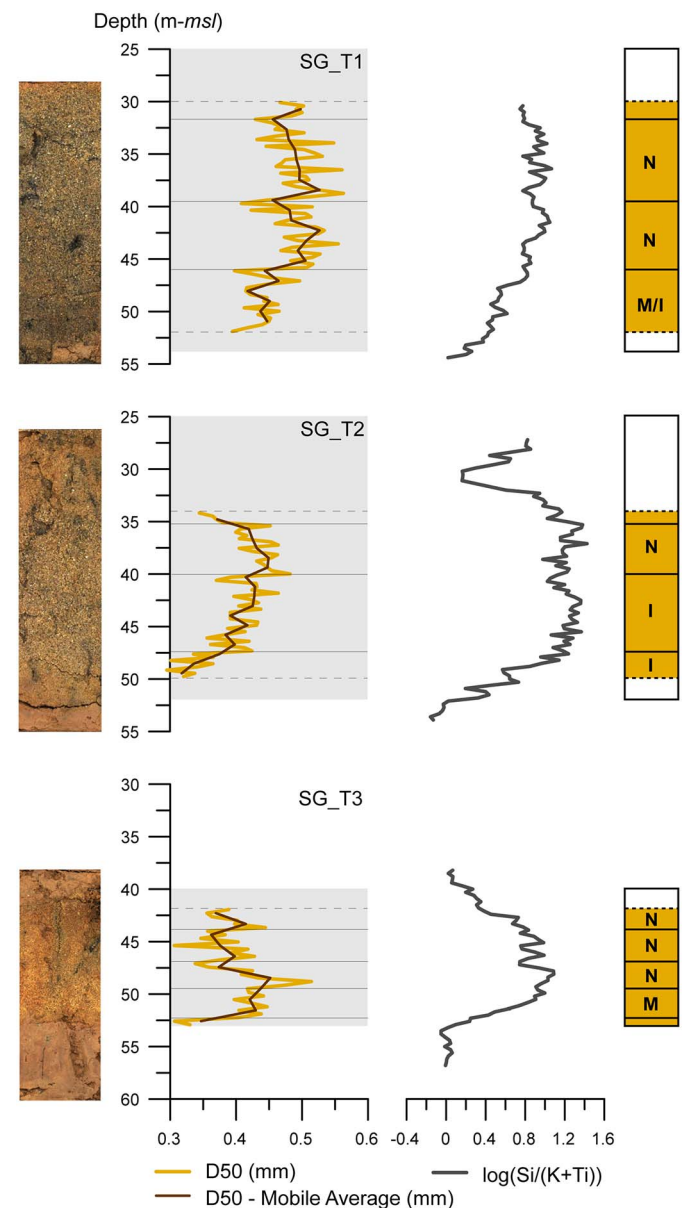


Fig. 5. High resolution images of box-cores SG_T1 to T3, sampled in the seaward section of the lagoonal basin. Vertical variation of median grain-size (D50), and respective moving average (three measurements), based on image analysis (IA), and of log-ratio Si/(K + Ti) within the sandy tsunami deposit (represented by the shaded area). Schematic interpretation of the identified sedimentary sequences (M — massive, N — normal graded, and I — inverse graded).

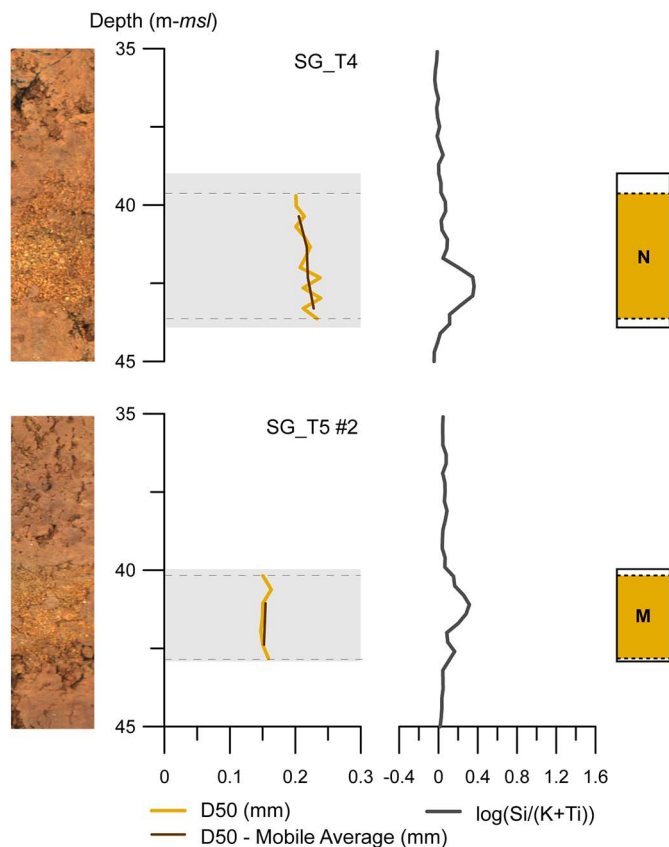


Fig. 6. High resolution images of box-cores SG_T4 and SG_T5#2, sampled in the landward section of the lagoonal basin. Vertical variation of median grain-size (D50), and respective moving average (three measurements), based on image analysis (IA), and of log-ratio Si/(K + Ti) within the sandy tsunami deposit (represented by the shaded area). Schematic interpretation of the identified sedimentary sequences (M — massive, N — normal graded, and I — inverse graded).

fining-upward sequence in the topmost 3 cm analyzed, whose median grain-size varies between 427 and 512 μm .

In SG_T2 the tsunami deposit (although only partially analyzed), shows: a) an inverse graded basal sequence up to 47.5 cm bs (4.5 cm thick), with median grain-size varying from 295 up to 365 μm , which is clearly finer than all overtopping sands; b) a second coarsening-upward

sequence, between 47.5 and 40.5 cm bs (7 cm thick), with coarser sand (356–464 μm); and c) a fining-upward sequence extending up to at least 34 cm bs (≥ 6.5 cm thick), with median grain-size range of 344 to 482 μm (Fig. 5). In the upper part of the tsunami sand, extending from 34 to 27 cm bs, incorporation of muddy material was observed macroscopically (either dispersed in sand or as mudballs), which renders IA unreliable. Hence, this part of the dataset was disregarded. However, field observations indicate that above 34 cm bs the sandy fraction of the event deposit is finer compared to the underlying tsunami sand.

The basal section of the tsunami deposit sampled in SG_T3 is composed by median sand (Fig. 5); however, it initiates with a thin and finer sequence (median grain-size of 307–330 μm), comprised between 53 and 52.5 cm bs, followed by a massive sequence, up to 49.5 cm bs, with fairly constant median grain-size (397–447 μm). Above 49.5 cm three fining-upward sequences were identified, separated at 47 and 43.5 cm bs, with thicknesses of 2.5, 3.5 and at least 2 cm, respectively. Within these three positive graded sequences, variability in median grain-size is higher in the lower sequence, and subsequently decreases in each of the following sequences.

The median grain-size of the sandy deposit (44 to 39.5 cm bs) in SG_T4 slightly decreases upwards, from 239 to 201 μm , thus showing a single fining-upward trend (Fig. 6), with the coarser particles confined below 42 cm bs.

In SG_T5#2 the tsunami deposit is characterized by fine sand, and the median grain-size is virtually constant throughout the sequence (ca. 153 μm) (Fig. 6).

5.4. Heavy minerals

The tsunami sand analyzed in three box-cores (SG_T1, SG_T2 and SG_T4) is generally low in HM contents (0.40–1.63%), with a decreasing trend towards the top and showing lower values inland (Table 2). An appreciable percentage of opaque grains [mainly magnetite and/or hematite according to Costa et al. (2015)] was observed, typically between 40 and 65%.

Overall, an increase in HM content is associated with coarser sediments (Fig. 7). Samples with lower HM contents (*i.e.* 0.4–0.6%) generally correspond to fine sand (228–272 μm). This correlation is evidenced by a linear relation between the percentage of magnetic (0.02–0.27%) and opaque minerals (0.2–1.1%) and mean grain-size (R ; Andrade et al., 2003) ≥ 0.85 (Fig. 7).

Among the transparent minerals observed were tourmaline,

Table 2
Heavy mineral assemblages of the studied samples from the tsunami sandy layer in the Salgados lagoon.

Box-core	Average depth (cm)	D50 (μm)	% relative to total sediment			% relative to transparent minerals								
			Heavy minerals			Tourmaline	Andalusite	Staurolite	Zircon	Pyroxenes	Amphiboles	Garnet	Titanite	Rutile
			Total	Magnetic	Opagues									
SG_T1	31.5	468.3	1.22	0.21	0.7	44.3	22.9	16.0	11.5	0.0	3.8	0.0	0.8	0.0
	33.5	512.4	1.43	0.18	0.8	39.5	24.2	21.8	7.3	1.6	3.2	0.8	1.6	0.0
	38.5	526.6	1.41	0.23	0.8	43.9	27.2	9.7	6.1	2.6	3.5	0.9	4.4	0.9
	41.5	530.7	1.51	0.23	0.9	43.9	22.3	13.9	6.2	7.7	0.0	1.5	3.9	0.8
	44.5	534.2	1.63	0.27	1.1	35.0	31.0	14.0	3.0	3.0	8.0	1.0	5.0	0.0
SG_T2	50.5	538.3	1.39	0.18	0.7	25.9	32.0	10.9	8.2	12.2	4.8	0.7	3.4	0.0
	27.5	241.2	0.56	0.03	0.3	42.1	33.6	8.6	4.3	5.7	2.1	0.7	2.1	0.0
	29.5	257.5	0.40	0.02	0.2	38.6	34.2	10.8	8.9	0.0	7.0	0.0	0.6	0.0
	33.5	485.4	1.44	0.20	0.8	49.6	18.8	17.3	6.0	6.8	0.0	1.5	0.0	0.0
	36.5	500.2	1.29	0.20	0.8	40.8	20.0	12.0	8.0	12.8	0.8	1.6	3.2	0.0
SG_T4	38.5	498.9	1.23	0.18	0.7	40.8	17.7	17.7	9.2	10.0	0.0	0.8	0.8	0.8
	42.5	480.1	1.18	0.15	0.7	48.8	25.2	11.8	4.7	0.8	6.3	0.8	0.8	0.0
	45.5	438.9	0.91	0.05	0.5	42.7	15.4	16.9	12.5	7.4	2.2	0.0	2.2	0.0
	39.5	228.2	0.40	0.02	0.2	35.8	37.8	8.0	4.6	2.0	9.3	1.3	0.0	0.7
	40.5	261.3	0.46	0.02	0.2	44.2	28.2	10.3	5.1	0.0	8.3	1.3	1.3	0.0
	41.5	271.5	0.56	0.03	0.2	36.8	29.2	11.9	4.3	10.8	2.7	1.6	0.0	0.0
	42.5	265.2	0.60	0.04	0.2	53.0	23.8	10.9	3.5	5.9	0.0	1.5	0.5	0.0

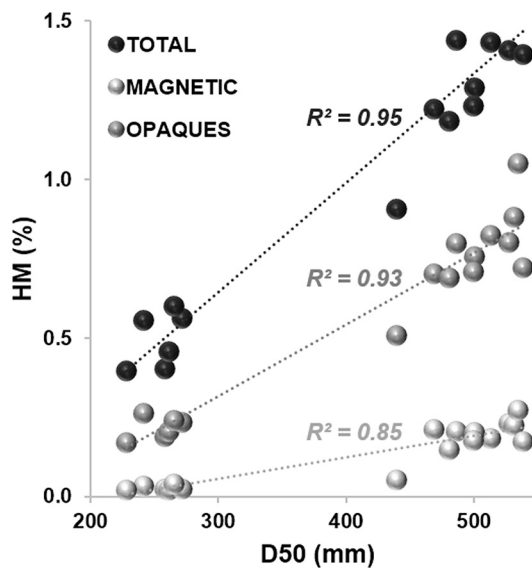


Fig. 7. Variation of the total percentage of heavy minerals, magnetic and opaque particles in total sediment fraction in function of the median grain-size (D50).

andalusite, staurolite, zircon, pyroxenes, amphiboles, garnet, titanite and rutile (Table 2). In all samples, tourmaline, andalusite and staurolite typically represent > 80% of the transparent HM assemblage. Zircon was observed in all samples, with values varying from 3 to 12.5%. Still, this result refers to the $1 < \Phi \leq 3$ ($125 \leq \mu\text{m} < 500$) fraction only. The very fine sand fraction ($63 \leq \mu\text{m} < 125$) was also analyzed semi-quantitatively for HM and results obtained revealed that both sand fractions present similar HM quantitative composition.

6. Discussion

6.1. Sandy tsunami deposit recognition and characterization

The deposit generated by the AD 1755 tsunami in the Salgados lagoon is characterized by sandy sediments with bioclasts (Costa et al., 2012a), the observed changes in Si/Al, Ca/Ti and K-, Ti- and Zr/total counts along the sedimentary columns allowed differentiation between tsunami and lagoonal sediments (Fig. 3). Variations in Si/Al reflect changes in mineral content of the sediment that are also reflected in textural features, whereas Ca/Ti reflects the calcium carbonate content. Higher values of both ratios indicate significant amounts of quartz and CaCO_3 , the latter mainly corresponding to shell hash or fragmented bioclasts. In contrast, low values of both Si/Al and Ca/Ti reflect fine-grained muddy sediments, with higher contents of aluminosilicates (e.g. clay minerals) and only trace amounts of bioclasts. The presence of rip-up clasts of mud entrained from the lagoonal bottom by the tsunami and mixed with sand of the event layer result in local decreases in Si/Al and Ca/Ti. This is observed, for example, in SG_T2 and SG_T5#2 at 29–31 and around 42 cm bs, respectively. The K-, Ti- and Zr/total counts ratios, generally showing lower values in the sandy tsunami sediments, also provide complementary information to identify the event layer in cases where there is pronounced textural contrast with the framing sediments (Fig. 3). All these three elements are associated with minerals (clays and phyllosilicates) which are more abundant in fine-grained sediments. The tsunami layer in box-cores SG_T4 and SG_T5#2 is relatively thin and varies in thickness. The tsunami deposit in both locations shows similar thickness, 1.5 to 4 cm and 1 to 3 cm, respectively, in spite the distance (ca. 220 m) separating both locations. This implies that the landward change in thickness of the event layer is non-linear, most of the change occurring closer to the coastline of the lagoonal basin, up to about 120 m from the leeward slope of the dune.

In some cases, the tsunami deposits show peaks of Ti- and Zr/total

counts potentially related to the presence of Ti and Zr-bearing minerals, such as rutile (TiO_2) and zircon (ZrSiO_4). In SG_T1 and T2, where the event layers are thicker, three and five Zr-peaks were respectively identified. Further inland, in SG_T3 and T4, where the deposit is thinner, just one peak of Zr was detected. In the case of SG_T3, the mentioned peak concurs with a high Ti value. HM assemblages at specific levels of the tsunami deposit shows that zircon and rutile maxima do not coincide with higher Zr and Ti/total counts. Potentially, individual XRF count peaks might be related to individual coarse grained zircon or rutile particles, directly under the XRF beam, resulting in a single high amplitude peak for these elements (Cúven et al., 2010). This implies that in coarser grained sediments, such as the tsunami deposits, post processing is necessary to filter out single peak maxima.

Despite geochemical normalization, the downcore variation of Cl, S and Br values slightly reflect the texture of sediments in box-cores from SG_T1 to SG_T5#2 (Fig. 3), where there is significant contrast in grain-size and composition between the event layer and the framing materials. This implies that either the Al-normalization does not fully compensate for changes in grain-size or there was an extra input of seawater. In box-cores SG_T1, T2 and T3, Al-normalized Cl, S and Br values show similar vertical variation profiles, with higher values within the sandy layer when compared to the lower values in the under and overlying sediments. Further inland, in box-core SG_T4 and SG_T5#2 vertical changes in Cl/Al and S/Al are similar, but Br/Al does not show any significant increase in relation with the tsunami layer. In the uppermost section of these two box-cores, within the lagoonal mud, peaks of Al-normalized Cl, S and Br values were detected (Fig. 3) (e.g. at 34.5 and 31.5 cm bs in SG_T4 and SG_T5#2, respectively). These maxima might reflect post-tsunami marine inundations (e.g. driven by storms or enhanced seawater input through the tidal inlet) or drought periods leading to temporary and significant increase in salt concentrations.

In contrast with previous studies addressing the geochemical imprint of tsunami inundations in terrestrial and freshwater environments (e.g. Chagué-Goff et al., 2012a,b; Andrade et al., 2003; Font et al., 2013), in the case of Salgados lowland the geochemical signature of the lagoonal muddy sediment is influenced by marine water, despite being also influenced by terrestrial sources. This is due to frequent connection of the lagoon with the ocean, conferring brackish to saline characteristics of the lagoonal water that translates into the geochemistry of the sediment.

6.2. Geochemical imprint beyond the tsunami sandy deposit

The AD 1755 tsunami inundation extent in the region of Salgados may be inferred from the historical record. Although no specific description focused in Salgados lowland (because there was no important village in the area), in the adjacent Alcantarilha lowland (approx. 2 km to the west — Fig. 1B) historical documents describe inundation as having reached up to 3 km inland “... leaving salty water lakes in the lowlands, creating islands and drowning 84 people” (Lopes, 1841). The geomorphological differences between the two adjacent areas are relevant, translating into differences in accommodation space: 2 km in Salgados and 3 km in Alcantarilha. Therefore, it is anticipated that the tsunami flooding extent in Salgados was somewhat smaller than in Alcantarilha.

According to Costa et al. (2012a) the sandy tsunami deposit extends 850 m inland from the present-day coastline in Salgados. Nevertheless, several studies suggested that the landward limit of a tsunami deposit underestimates the inundation extent (e.g. Gelfenbaum and Jaffe, 2003; MacInnes et al., 2009; Goto et al., 2011; Morton et al., 2011; Abe et al., 2012; Chagué-Goff et al., 2015, 2017). The relation between the maximum inundation distance and the inland extent of tsunami deposit depends on several factors such as the waves' characteristics, the geomorphological setting and sediment availability. The limit of the inundation extent can be traced using salinity indicators such as Cl, S and

Br, especially in fine and/or organic-rich sediments which have a higher potential to preserve these geochemical signals/elements. This was highlighted by Chagué-Goff et al. (2012a,b) based on studies conducted on the Sendai Plain after the Tohoku-oki tsunami, where the extent of the tsunami sand and mud (up to 2.9 and 4.65 km inland, respectively) corresponded to 60 to nearly 95% of the maximum tsunami inundation, respectively. Furthermore, in a post-tsunami survey, seven months after the impact, S and Cl markers were well preserved in the muddy sediments and underlying soil, far beyond the limit of the recognizable sand deposit (Chagué-Goff et al., 2012a,b).

In Lagoa dos Salgados, the tsunami deposit in trench SG_T5 becomes strongly irregular and disappears within the mud. In box-core SG_T5#2 the sandy layer is still macroscopically recognizable with an average thickness of 2 cm, but in SG_T5#1 (located app. 10 m further north) textural homogeneity is observed (Fig. 3). The Al-normalized ratios of Cl, S and Br in box-core SG_T5#1 show an overall decreasing trend towards the top (Fig. 3). These salinity indicators tend to occur in higher proportions deeper than 38 cm *bs*, where some peaks of these ratios are identifiable. Although the total number of peaks differs, they coincide at the same depths: ca. 40, 42 and 45 cm *bs*, suggesting ephemeral and pronounced changes in the salinity of the lagoonal environment. The depth range of these peaks roughly matches the adjacent tsunami deposit observed in SG_T5#2 (Fig. 3) and are interpreted as related with the massive input of marine water due to the AD 1755 tsunami inundation.

6.3. Distinctive inundation phases

The texture of the AD 1755 tsunami deposit in the Salgados lowland is essentially massive under macroscopic observation (Costa et al., 2012a), although most historical records indicate three subsequent waves flooding the Algarve lowlands (e.g. Mendonça, 1758). The textural and geochemical data gathered along the tsunami layer with IA and XRF core-scanning were combined to look for evidences of signatures of inundation and backwash phases.

Primarily, grain-size IA provided evidences that the tsunami deposit is not truly massive. The vertical grain-size variations observed in different sampling locations suggest that the seaward box-cores (SG_T1 to T3) preserve more information on tsunami depositional phases than the landward box-cores (SG_T4 to T5#2) (Figs. 5 and 6). In the seaward box-cores (SG_T1 to T3) the tsunami layer consists of at least four superimposed sand packages (Fig. 5), whereas in SG_T4 and T5#2 only one package can be identified (Fig. 6). Based solely on the number of sedimentary sequences detected, the seaward locations experienced a higher number of tsunami inundation phases.

Regardless the number of phases in each box-core, it is clear that in SG_T1 to SG_T3 the basal part of the tsunami deposit presents one (or two) massive or inversely graded sequences — identified using IA (Figs. 5 and 6). Following these basal sequences, three normal graded sequences are identified by IA analysis in SG_T1 and SG_T3 (Figs. 6 and 7). However, in SG_T2 only one fining-upward sequence is identified using IA. This is due to the sampling constraints in this box-core — the deposit was not fully sampled. On the other hand, in both inland box-cores only one depositional sequence is recognized. This sequence shows normal grading in SG_T4 and in SG_T5#2 the absence of a clear grain-size trend is interpreted as resulting from post-depositional reworking of an extremely thin and irregular layer. This implies that apparently not all the inundation phases reached the inner part of the lagoonal basin or, if they did so, their energy was not sufficient to transport coarser sediments to the more inland sector of the basin. In any case, these results are in agreement with the geochemical data (Cl and Br), showing that the grain-size signal only captures part of the tsunamigenic inundation extent.

The detailed examination of the small-scale variation in grain-size allows identification of different tsunami sediment transport modes (Jaffe et al., 2012). Typically, inverse or massive sedimentary

sequences occur on the basal section of tsunami layers and are consistent with bedload-dominated transport and deposition (Moore et al., 2011). The upper portion of the tsunami layers usually results from suspended-load processes and typically produces normally graded sequences, the deposition being controlled by size, density and shape of the particles (Jaffe et al., 2012 and references therein). However, bedload associated deposition has also been found in the topmost section of tsunami laminated deposits (Szczuciński, 2012). The thickness of each fining-upwards sequence depends on the amount of sediment available in suspension (Jaffe and Gelfenbaum, 2007).

In our study case the massive or inverse graded basal sequence found in the seaward box-cores (up to ~500 m from present-day coastline) suggests the dominance of bedload transport during the initial phases of the AD 1755 tsunami inundation in that sector of the basin. In tsunamis, bedload transport is associated with high flow velocities and high density sediment load (Jaffe et al., 2012).

The characteristics of basal package are congruent with the earliest overwash of the coastal dunes and with maximum incorporation of sediments from the coastal system, generating a localized peak in sediment concentration. In fact, previous studies have shown that most of the AD 1755 tsunami sand deposited in Salgados and elsewhere in the Algarve coast was sourced from well-sorted coastal dune sand and secondarily in somewhat coarser beach sands (Hindson and Andrade, 1999; Costa et al., 2012a, 2015). Furthermore, the study by Costa et al. (2016) shows that the maximum erosive potential of the AD 1755 inundation in Salgados is located in the leeward slope of the coastal dunes and that deposition starts at a short distance further inland. Due to high sediment concentration in this region, massive or inversely graded deposits occur (they can be recognized in SG_T1 to SG_T3) and are controlled by flow deceleration and decreasing sediment availability in landward direction.

The very fact that the basal package(s) is a distinctive stratigraphic feature implies that the governing conditions did not repeat in time, thus subsequent inundation phases transported less sediment either due to lower flow velocities or lower sediment availability in the coastal system. This is later translated in sedimentary packages showing normal grading. The number of packages overlying the basal one is virtually consistent throughout the seaward section of the tsunami deposit. A contrasting number of depositional phases are found in the literature associated with the AD 1755 tsunami in southern Iberia using different sedimentological, palaeoecological and geochemical proxies. An extensive survey of Boca do Rio alluvial plain sediments (Algarve, Portugal), presented in Hindson and Andrade (1999), indicate five sedimentologically distinct sub-units within the tsunami sand layer in the more seaward sampling sites. The detailed stratigraphic analysis of the trenches excavated at that location suggested more than one episode of sedimentation within the AD 1755 tsunami layer, especially evident in the more seaward portion of the lowland. Based on the study of sediment retrieved from three trenches in the Alcantarilha alluvial plain, Quintela et al. (2016) were able to differentiate three distinct sediment transport phases within the AD 1755 tsunami sediment unit, relying mostly on the study of foraminifera assemblages. However, the tsunami layer deposited by the same event at Los Lances coastal plain (SW Spain) was, by coupling high-resolution textural and geochemical analysis, internally subdivided into 8 or 10 distinct subunits (Cuven et al., 2013; Falvard and Paris, 2016). However, the sedimentary record was considered as being incomplete due to reworking and erosion during the tsunami itself.

To establish correlation between the number of tsunami waves and depositional phases an unequivocal evidence of backwash must be identified in the sedimentary record. This can be performed using either textural (e.g. Mhammedi et al., 2015; Kain et al., 2016), paleontological (e.g. Sawai et al., 2009; Quintela et al., 2016) or compositional proxies (e.g. Jagodziński et al., 2009, 2012). In conceptual terms, inundation phases of the study area addressed in this study should be responsible for the input of sediments richer in Si and Ca (quartz and bioclastic

dune and beach sands), whereas the backwash may be responsible for entrainment and transport of terrestrial-sourced sediments richer in Al, Ti and Fe, in agreement with the composition of hinterland sources.

In our studied case, textural and geochemical data were inconclusive regarding this aspect of the inundation. Furthermore, macroscopic analysis of the trench walls and box-cores shows that the transition between contiguous sand packages is continuous, with no traces of mud drapes or any other evidences of finer sedimentation separating inrush phases of marine water. Thus, there are no sedimentological imprints testifying for the transient point immediately preceding flow inversion or separating two successive incoming waves. We hypothesize that the reasons underlying this result rest on the inability of the backflow to transport and redeposit land-sourced material on the surveyed region of the lowland. Indeed, as previously described in the 2011 Tohoku-oki tsunami, the backflow tends to be channelized (Chagué-Goff et al., 2012b; Richmond et al., 2012; Sugawara et al., 2014), thus the correspondent sedimentary imprint should be spatially restricted.

Cuven et al. (2010) established correlation between geochemistry and grain-size (Si — quartz sand and coarse silts; Ti — silts; K — clays). We combined our geochemical data to investigate to what extent the vertical variation of the ratio $Si/(K + Ti)$ within the tsunami sands correlates with the grain-size data derived from IA (Figs. 5 and 6). The results show that both datasets are in good agreement. In the basal packages, the vertical downcore profile of that ratio is broadly uniform as expected in a mixture showing no relevant size grading. In opposition, each identified normal graded sequence shows an upward decrease of that ratio, mimicking the trend in the grain-size. The range of the grain-size variations in each box-core is small due to well-sorted sediment sources (beach and dune) and this also reflects in the small amplitude of the geochemical signal. In this case, the vertical variation of the geochemical index within each package results from the flow deceleration creating conditions for the deposition of minor amounts of smaller quartz particles and lighter and platy mica and clay particles in the topmost region of each package.

The results produced and discussed herein stress the importance of coupling high-resolution geochemical and grain-size analysis when interpreting the depositional signature of tsunamis. The combination of both methods allowed discriminating different inundation phases that are schematically represented in the conceptual model presented in Fig. 8. Those would be overseen, if discrete samples taken at lower resolution (e.g. each centimeter) had been used.

7. Conclusions

In the work presented here we demonstrated that geochemical data (mainly Si/Al and Ca/Ti) allows the precise determination of the lower and upper limits of the sandy deposit associated with the AD 1755 tsunami, even when that contact is not obvious macroscopically.

Geochemical salinity indicators, such as Cl and Br, were detected beyond the sandy sedimentological signature thus, indicating that the marine inundation extended farther than the deposit and that 260 years after the event its geochemical signature is still preserved in lagoonal stratigraphy, despite the permanent sediment regime in a saline to brackish environment.

The use of high-resolution IA (median grain-size) and elemental XRF analysis ($Si/(K + Ti)$) allowed discriminating, at least four different inundation phases within the sandy tsunami deposit in the seaward region subjected to the inundation, whereas in the landward region only one phase can be identified. The lowermost massive or coarsening-upwards sequence(s) is usually finer than the overlying sequences, showing lower values of $Si/(K + Ti)$ and probably corresponding to bedload transport in a high sediment concentration flow. By contrast, the following packages are normally graded and settled from graded suspension, indicating, lower flow velocities and less sediment incorporation in the water column.

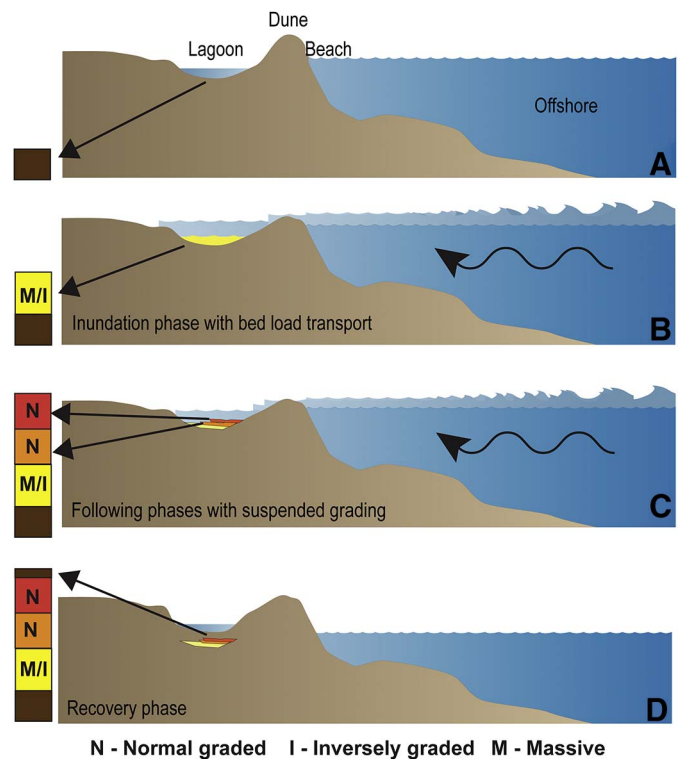


Fig. 8. Conceptual model of the deposition of sedimentary sequences (M — massive, N — normal graded, and I — inverse graded) associated with the AD 1755 tsunami in Salgados Lagoon.

The small range in variations of median grain-size and $Si/(K + Ti)$ is a consequence of a well-sorted and both texturally and compositionally mature source area (beach and dune sand). In fact, both geochemical and grain-size data were inconclusive regarding clear-cut identification of backwash phases of the tsunami, which could input a wider textural and compositional signal in the tsunami sands. This is interpreted as representing less transport competence or localized deposition within the flooded area.

This study shows the relevance of combining high-resolution geochemical and grain-size investigations in coastal sequences to improve reconstruction of the inundation extent, where no significant textural contrast exists between the event and the typical sedimentation regime. Moreover, this combined approach provided innovative insights in our capability to resolve coarse clastic tsunami sediments for different modes of transport and inundation pulses.

Acknowledgements

The authors are thankful to J.P. Cascalho, T. Silva and R. Gieles for their help during field and laboratory work. P. Costa and C. Ponte Lira acknowledge support from FCT Post-Doctoral Grants (SFRH/BPD/84165/2012 and SFRH/BPD/81800/2011, respectively). Authors benefited from support from project GETS (FCT-PTDC/CTE-GEX/65948/2006). This work had the contribution of the project FCT UID/GEO/50019/2013 — Instituto Dom Luiz. The authors would like to acknowledge the very constructive comments provided by Witold Szczucinski and another anonymous reviewer.

References

- Abe, T., Goto, K., Sugawara, D., 2012. Relationship between the maximum extent of tsunami sand and the inundation limit of the 2011 Tohoku-oki tsunami on the Sendai Plain, Japan. *Sediment. Geol.* 282, 142–150. <http://dx.doi.org/10.1016/j.sedgeo.2012.05.004>.
- Andrade, C., Freitas, M., Miranda, J., 2003. Recognizing possible tsunami sediments in the ultradissipative environment of the Tagus estuary (Portugal). In: Davis, R.A.,

- Sallenger, A., Howd, P. (Eds.), *Coastal Sediments' 03 — The 5th International Symposium on Coastal Engineering and Science of Coastal Sediments Processes*. Clearwater Beach, Florida, pp. 1–14.
- Atwater, B.F., 1987. Evidence for great Holocene earthquakes along the outer coast of Washington State. *Science* 236 (4804), 942–944. <http://dx.doi.org/10.1126/science.236.4804.942>.
- Atwater, B.F., ten Brink, U.S., Buckley, M., Halley, R.S., Jaffe, B.E., López-Venegas, A.M., Reinhardt, E.G., Tuttle, M.P., Watt, S., Wei, Y., 2012. Geomorphic and stratigraphic evidence for an unusual tsunami or storm a few centuries ago at Anegada, British Virgin Islands. *Nat. Hazards* 63 (1), 51–84. <http://dx.doi.org/10.1007/s11069-010-9622-6>.
- Baptista, M.A., Heitor, S., Miranda, J.M., Miranda, P., Victor, L.M., 1998. The 1755 Lisbon tsunami; evaluation of the tsunami parameters. *J. Geodyn.* 25, 143–157. [http://dx.doi.org/10.1016/S0264-3707\(97\)00019-7](http://dx.doi.org/10.1016/S0264-3707(97)00019-7).
- Baptista, M.A., Miranda, J.M., Chierici, F., Zitellini, N., 2003. New study of the 1755 earthquake source based on multi-channel seismic survey data and tsunami modeling. *Nat. Hazards Earth Syst. Sci.* 3, 333–340. <http://dx.doi.org/10.5194/nhess-3-333-2003>.
- Barkan, R., ten Brink, U.S., Lin, J., 2009. Far field tsunami simulations of the 1755 Lisbon earthquake: implications for tsunami hazard to the U.S. East Coast and the Caribbean. *Mar. Geol.* 264, 109–122. <http://dx.doi.org/10.1016/j.margeo.2008.10.010>.
- Benson, B.E., Grimm, K.A., Clague, J.J., 1997. Tsunami deposits beneath tidal marshes on northwestern Vancouver Island, British Columbia. *Quat. Res.* 48, 192–204. <http://dx.doi.org/10.1006/qres.1997.1911>.
- Bondevik, S., Svendsen, J.I., Mangerud, J., 1997. Tsunami sedimentary facies deposited by the Storegga tsunami in shallow marine basins and coastal lakes, western Norway. *Sedimentology* 44, 1115–1131. <http://dx.doi.org/10.1046/j.1365-3091.1997.d01-63.x>.
- Brumsack, H.-J., 2006. The trace metal content of recent organic carbon-rich sediments: implications for Cretaceous black shale formation. *Palaeogeogr. Palaeoclimatol. Palaeoecol.* 232, 344–361. <http://dx.doi.org/10.1016/j.palaeo.2005.05.011>.
- Buscombe, D., 2013. Transferable wavelet method for grain-size distribution from images of sediment surfaces and thin sections, and other natural granular patterns. *Sedimentology* 60 (7), 1709–1732. <http://dx.doi.org/10.1111/sed.12049>.
- Chagué-Goff, C., Schneider, J.-L., Goff, J.R., Dominey-Howes, D., Strotz, L., 2011. Expanding the proxy toolkit to help identify past events — lessons from the 2004 Indian Ocean Tsunami and the 2009 South Pacific Tsunami. *Earth Sci. Rev.* 107, 107–122. <http://dx.doi.org/10.1016/j.earscirev.2011.03.007>.
- Chagué-Goff, C., Andrew, A., Szczuciński, W., Goff, J., Nishimura, Y., 2012a. Geochemical signatures up to the maximum inundation of the 2011 Tohoku-oki tsunami — implications for the 869AD Jogan and other palaeotsunamis. *Sediment. Geol.* 282, 65–77. <http://dx.doi.org/10.1016/j.sedgeo.2012.05.021>.
- Chagué-Goff, C., Niedzielski, P., Wong, H.K.Y., Szczuciński, W., Sugawara, D., Goff, J., 2012b. Environmental impact assessment of the 2011 Tohoku-oki tsunami on the Sendai Plain. *Sediment. Geol.* 282, 175–187. <http://dx.doi.org/10.1016/j.sedgeo.2012.06.002>.
- Chagué-Goff, C., Goff, J., Wong, H.K.Y., Cisternas, M., 2015. Insights from geochemistry and diatoms to characterise a tsunami's deposit and maximum inundation limit. *Mar. Geol.* 359, 22–34. <http://dx.doi.org/10.1016/j.margeo.2014.11.009>.
- Chagué-Goff, C., Szczuciński, W., Shinozaki, T., 2017. Applications of geochemistry in tsunami research: A review. *Earth Sci. Rev.* 165, 203–244.
- Costa, P.J.M., Andrade, C., Freitas, M., Oliveira, M., Lopes, V., Dawson, A., Moreno, J., Fatela, F., Jouanneau, J.-M., 2012a. A tsunami record in the sedimentary archive of the central Algarve coast, Portugal: characterizing sediment, reconstructing sources and inundation paths. *The Holocene* 22, 899–914. <http://dx.doi.org/10.1177/0959683611434227>.
- Costa, P.J.M., Andrade, C., Dawson, A.G., Mahaney, W.C., Freitas, M.C., Paris, R., Taborda, R., 2012b. Microtextural characteristics of quartz grains transported and deposited by tsunamis and storms. *Sediment. Geol.* 275, 55–69. <http://dx.doi.org/10.1016/j.sedgeo.2012.07.013>.
- Costa, P.J.M., Andrade, C., Cascalho, J., Dawson, A.G., Freitas, M.C., Paris, R., Dawson, S., 2015. Onshore tsunami sediment transport mechanisms inferred from heavy mineral assemblages. *The Holocene* 25, 795–809. <http://dx.doi.org/10.1177/0959683615569322>.
- Costa, P.J.M., Costas, S., González-Villanueva, R., Oliveira, M.A., Roelvink, D., Andrade, C., Freitas, M.C., Cunha, P.P., Martins, A., Buylaert, J.-P., Murray, A., 2016. How did the AD 1755 tsunami impact on sand barriers across the southern coast of Portugal? *Geomorphology* 268, 296–311. <http://dx.doi.org/10.1016/j.geomorph.2016.06.019>.
- Cuven, S., Francus, P., Lamoureux, S.F., 2010. Estimation of grain size variability with micro X-ray fluorescence in laminated lacustrine sediments, Cape Bounty, Canadian High Arctic. *J. Paleolimnol.* 44 (3), 803–817. <http://dx.doi.org/10.1007/s10933-010-9453-1>.
- Cuven, S., Paris, R., Falvard, S., Miot-Noirault, E., Benbakkar, M., Schneider, J.-L., Billy, I., 2013. High-resolution analysis of a tsunami deposit: case-study from the 1755 Lisbon tsunami in southwestern Spain. *Mar. Geol.* 337, 98–111. <http://dx.doi.org/10.1016/j.margeo.2013.02.002>.
- Dawson, A.G., Long, D., Smith, D.E., 1988. The Storegga Slides: evidence from eastern Scotland for a possible tsunami. *Mar. Geol.* 82 (3–4), 271–276. [http://dx.doi.org/10.1016/0025-3227\(88\)90146-6](http://dx.doi.org/10.1016/0025-3227(88)90146-6).
- Etienne, S., Buckley, M., Paris, R., Nandasena, A.K., Clark, K., Strotz, L., Chagué-Goff, C., Goff, J., Richmond, B., 2011. The use of boulders for characterising past tsunamis: lessons from the 2004 Indian Ocean and 2009 South Pacific tsunamis. *Earth Sci. Rev.* 107, 76–90. <http://dx.doi.org/10.1016/j.earscirev.2010.12.006>.
- Falvard, S., Paris, R., 2016. X-ray tomography of tsunami deposits: towards a new depositional model of tsunami deposits. *Sedimentology*. <http://dx.doi.org/10.1111/sed.12310>.
- Folk, R.L., Ward, W.C., 1957. Brazos River Bar — a study in the significance of grain size parameters. *J. Sediment. Petrol.* 27 (1), 3–26.
- Font, E., Veiga-Pires, C., Pozo, M., Nave, S., Costas, S., Ruiz Muñoz, F., Abad, M., Simões, N., Duarte, S., Rodríguez-Vidal, J., 2013. Benchmarks and sediment source(s) of the 1755 Lisbon tsunami deposit at Boca do Rio Estuary. *Mar. Geol.* 343, 1–14. <http://dx.doi.org/10.1016/j.margeo.2013.06.008>.
- Gelfenbaum, G., Jaffe, B., 2003. Erosion and sedimentation from the 17 July, 1998 Papua New Guinea Tsunami. *Pure Appl. Geophys.* 160, 1969–1999. <http://dx.doi.org/10.1007/s00024-003-2416-y>.
- Goff, J., Chagué-Goff, C., Nichol, S., Jaffe, B., Dominey-Howes, D., 2012. Progress in palaeotsunami research. *Sediment. Geol.* 243–244, 70–88. <http://dx.doi.org/10.1016/j.sedgeo.2011.11.002>.
- Goto, K., Chagué-Goff, C., Fujino, S., Goff, J., Jaffe, B., Nishimura, Y., Richmond, B., Sugawara, D., Szczuciński, W., Tappin, D.R., Witter, R.C., Yulianto, E., 2011. New insights of tsunami hazard from the 2011 Tohoku-oki event. *Mar. Geol.* 290, 46–50. <http://dx.doi.org/10.1016/j.margeo.2011.10.004>.
- Goto, K., Hashimoto, K., Sugawara, D., Yanagisawa, H., Abe, T., 2014. Spatial thickness variability of the 2011 Tohoku-oki tsunami deposits along the coastline of Sendai Bay. *Mar. Geol.* 358, 38–48. <http://dx.doi.org/10.1016/j.margeo.2013.12.015>.
- Grandin, R., Borges, J.F., Bezeghoud, M., Caldeira, B., Carrilho, F., 2007. Simulations of strong ground motion in SW Iberia for the 1969 February 28 (Ms = 8.0) and the 1755 November 1 (M = 8.5) earthquakes — II. Strong ground motion simulations. *Geophys. J. Int.* 171, 807–822. <http://dx.doi.org/10.1111/j.1365-246X.2007.03571.x>.
- Gutscher, M.-A., Baptista, M.A., Miranda, J.M., 2006. The Gibraltar Arc seismogenic zone (part 2): constraints on a shallow east dipping fault plane source for the 1755 Lisbon earthquake provided by tsunami modeling and seismic intensity. *Tectonophysics* 426, 153–166. <http://dx.doi.org/10.1016/j.tecto.2006.02.025>.
- Hindson, R.A., Andrade, C., 1999. Sedimentation and hydrodynamic processes associated with the tsunami generated by the 1755 Lisbon earthquake. *Quat. Int.* 56, 27–38. [http://dx.doi.org/10.1016/S1040-6182\(98\)00014-7](http://dx.doi.org/10.1016/S1040-6182(98)00014-7).
- Jaffe, B.E., Gelfenbaum, G., 2007. A simple model for calculating tsunami flow speed from tsunami deposits. *Sediment. Geol.* 200, 347–361. <http://dx.doi.org/10.1016/j.sedgeo.2007.01.013>.
- Jaffe, B.E., Goto, K., Sugawara, D., Richmond, B.M., Fujino, S., Nishimura, Y., 2012. Flow speed estimated by inverse modeling of sandy tsunami deposits: results from the 11 March 2011 tsunami on the coastal plain near the Sendai Airport, Honshu, Japan. *Sediment. Geol.* 282, 90–109. <http://dx.doi.org/10.1016/j.sedgeo.2012.09.002>.
- Jagodźński, R., Sternal, B., Szczuciński, W., Lorenc, S., 2009. Heavy minerals in 2004 tsunami deposits on Kho Khao Island, Thailand. *Pol. J. Environ. Stud.* 18, 103–110. <http://dx.doi.org/10.1007/s11069-011-9729-4>.
- Jagodźński, R., Sternal, B., Szczuciński, W., Chagué-Goff, C., Sugawara, D., 2012. Heavy minerals in the 2011 Tohoku-oki tsunami deposits — insights into sediment sources and hydrodynamics. *Sediment. Geol.* 282, 57–64. <http://dx.doi.org/10.1016/j.sedgeo.2012.07.015>.
- Kain, C.L., Wassmer, P., Goff, J., Chagué-Goff, C., Gomez, C., Hart, D.E., Fierro, D., Jacobsen, G.E., Zawadzki, A., 2016. Determining flow patterns and emplacement dynamics from tsunami deposits with no visible sedimentary structure. *Earth Surf. Process. Landf.* <http://dx.doi.org/10.1002/esp.4020>.
- Lira, C., 2011. Development of New Image Analysis Methodologies for Morphometric Characterization of Sediments. IST, Universidade Técnica de Lisboa <http://dx.doi.org/10.13140/RG.2.1.4685.9681>.
- Lira, C., 2015. High-resolution textural analysis of extreme wave event deposits. In: *INQUA 2015 — Quaternary Perspectives on Climate Change, Natural Hazards and Civilization*, (T00546-T01).
- Lira, C., Pina, P., 2007. Sedimentological analysis of sands. In: Martí, J., Benedí, J.M., Mendonça, A.M., Serrat, J. (Eds.), *Pattern Recognition and Image Analysis*. Third Iberian Conference, IbPRIA 2007, Girona, Spain, June 6–8, 2007, Proceedings, Part II Springer Berlin Heidelberg, Berlin, Heidelberg, pp. 388–395. http://dx.doi.org/10.1007/978-3-540-72849-8_49.
- Lopes, J.B.L.S., 1841. *Corografia ou Memória Económica, Estatística e Topográfica do Reino do Algarve*. Lisboa. (In Portuguese).
- Löwemark, L., Chen, H.-F., Yang, T.-N., Kylander, M., Yu, E.-F., Hsu, Y.-W., Lee, T.-Q., Song, S.-R., Jarvis, S., 2011. Normalizing XRF-scanner data: a cautionary note on the interpretation of high-resolution records from organic-rich lakes. *J. Asian Earth Sci.* 40, 1250–1256. <http://dx.doi.org/10.1016/j.jseae.2010.06.002>.
- MacInnes, B.T., Bourgeois, J., Pinegina, T.K., Kravchunovskaya, E.A., 2009. Tsunami geomorphology: erosion and deposition from the 15 November 2006 Kuril Island tsunami. *Geology* 37, 995–998. <http://dx.doi.org/10.1130/G30172A.1>.
- Mendonça, J.J.M., 1758. *Historia Universal dos Terremotos, que tem havido no mundo, de que ha noticia, desde a sua criação até o seculo presente*. Off. de Antonio Vicente da Silva (In Portuguese).
- Mhammedi, N., Medina, F., Trentesaux, A., Font, E., Belkhaty, Z., Geawhari, M.-A., 2015. Sedimentary evidence of palaeo-tsunami deposits along the Loukkos estuary (Moroccan Atlantic coast). *Sci. Tsunami Hazards* 34 (2), 83–100.
- Moore, A., Goff, J., McAdoo, B.G., Fritz, H.M., Gusman, A., Kalligeris, N., Kalsum, K., Susanto, A., Suteja, D., Synolakis, C.E., 2011. Sedimentary deposits from the 17 July 2006 western Java tsunami, Indonesia: use of grain size analyses to assess tsunami flow depth, speed, and traction carpet characteristics. *Pure Appl. Geophys.* 168, 1951–1961. <http://dx.doi.org/10.1007/s00024-011-0280-8>.
- Morton, R.A., Gelfenbaum, G., Buckley, M.L., Richmond, B.M., 2011. Geological effects and implications of the 2010 tsunami along the central coast of Chile. *Sediment. Geol.* 242, 34–51. <http://dx.doi.org/10.1016/j.sedgeo.2011.09.004>.
- Moura, D., Veiga-Pires, C., Albardeiro, L., Boski, T., Rodrigues, A.L., Tareco, H., 2007. Holocene sea level fluctuations and coastal evolution in the central Algarve (southern Portugal). *Mar. Geol.* 237, 127–142. <http://dx.doi.org/10.1016/j.margeo.2006.10.026>.

- Nomegaya, Y., Satake, K., 2014. Reexamination of the A.D. 869 Jogan earthquake size from tsunami deposit distribution, simulated flow depth, and velocity. *Geophys. Res. Lett.* 41, 2297–2303. <http://dx.doi.org/10.1002/2013GL058678>.
- Oliveira, C.S., 2005. Descrição do terramoto de 1755, sua extensão, causas e efeitos. O sismo. O tsunami. O incêndio. In: FLAD, Público (Ed.), *O Grande Terramoto de Lisboa. Descrições*, vol. 1. Tipografia Peres, SA, pp. 23–87 (In Portuguese).
- Paris, R., Fournier, J., Poizot, E., Etienne, S., Morin, J., Lavigne, F., Wassmer, P., 2010. Boulder and fine sediment transport and deposition by the 2004 tsunami in Lhok Nga (western Banda Aceh, Sumatra, Indonesia): a coupled offshore–onshore model. *Mar. Geol.* 268, 43–54. <http://dx.doi.org/10.1016/j.margeo.2009.10.011>.
- Pina, P., Lira, C., Lousada, M., 2011. In-situ computation of granulometries of sedimentary grains — some preliminary results. *J. Coast. Res. SI* (64), 1727–1730.
- Quintela, M., Costa, P.J.M., Fatela, F., Drago, T., Hoska, N., Andrade, C., Freitas, M.C., 2016. The AD 1755 tsunami deposits onshore and offshore of Algarve (south Portugal): sediment transport interpretations based on the study of foraminifera assemblages. *Quat. Int.* 408, 123–138. <http://dx.doi.org/10.1016/j.quaint.2015.12.029>.
- Richmond, B., Szczuciński, W., Chagué-Goff, C., Goto, K., Sugawara, D., Witter, R., Tappin, D.R., Jaffe, B., Fujino, S., Nishimura, Y., Goff, J., 2012. Erosion, deposition and landscape change on the Sendai coastal plain, Japan, resulting from the March 11, 2011 Tohoku-oki tsunami. *Sediment. Geol.* 282, 27–39. <http://dx.doi.org/10.1016/j.sedgeo.2012.08.005>.
- Richter, T.O., van der Gaast, S., Koster, B., Vaars, A., Giele, R., de Stigter, H.C., De Haas, H., van Weering, T.C.E., 2006. The Avaatech XRF core scanner: technical description and applications to NE Atlantic sediments. *Geol. Soc. Lond., Spec. Publ.* 267, 39–50. <http://dx.doi.org/10.1144/GSL.SP.2006.267.01.03>.
- Rothwell, G., Croudace, I.W., 2015. Twenty years of XRF core scanning marine sediments: what do geochemical proxies tell us? In: Rothwell, I.W.C., R. G. (Eds.), *Micro-XRF Studies of Sediment Cores — Applications of a Non-destructive Tool for the Environmental Sciences*. Springer, Dordrecht, Netherlands, pp. 25–102.
- Sawai, Y., Jankaew, K., Martin, M.E., Prendergast, A., Choowong, M., Charoentitrat, T., 2009. Diatom assemblages in tsunami deposits associated with the 2004 Indian Ocean tsunami at Phra Thong Island, Thailand. *Mar. Micropaleontol.* 73, 70–79. <http://dx.doi.org/10.1016/j.marmicro.2009.07.003>.
- Sousa, F.L.P., 1919. O terremoto do 1º de Novembro de 1755 em Portugal e um estudo demográfico: Distritos de Faro, Beja e Évora. Volume I. Serviços Geológicos. Tipografia do Comércio, Lisboa (In Portuguese).
- Sugawara, D., Minora, K., Imamura, F., 2008. Tsunamis and tsunami sedimentology. In: Shiki, T., Tsuji, Y., Yamazaki, T., Minoura, K. (Eds.), *Tsunamiites — Features and Implications*. Elsevier, pp. 9–49.
- Sugawara, D., Goto, K., Imamura, F., Matsumoto, H., Minoura, K., 2012. Assessing the magnitude of the 869 Jogan tsunami using sedimentary deposits: prediction and consequence of the 2011 Tohoku-oki tsunami. *Sediment. Geol.* 282, 14–26. <http://dx.doi.org/10.1016/j.sedgeo.2012.08.001>.
- Sugawara, D., Takahashi, T., Imamura, F., 2014. Sediment transport due to the 2011 Tohoku-oki tsunami at Sendai: results from numerical modeling. *Mar. Geol.* 358, 18–37. <http://dx.doi.org/10.1016/j.margeo.2014.05.005>.
- Szczuciński, W., 2012. The post-depositional changes of the onshore 2004 tsunami deposits on the Andaman Sea coast of Thailand. *Nat. Hazards* 60, 115–133. <http://dx.doi.org/10.1007/s11069-011-9956-8>.
- Tappin, D.R., Evans, H.M., Jordan, C.J., Richmond, B., Sugawara, D., Goto, K., 2012. Coastal changes in the Sendai area from the impact of the 2011 Tōhoku-oki tsunami: interpretations of time series satellite images, helicopter-borne video footage and field observations. *Sediment. Geol.* 282, 151–174. <http://dx.doi.org/10.1016/j.sedgeo.2012.09.011>.
- Tjallingii, R., 2006. Application and Quality of X-ray Fluorescence Core Scanning in Reconstructing Late Pleistocene NW African Continental Margin Sedimentation Patterns and Paleoclimate Variations. Universität Bremen.
- Tjallingii, R., Röhl, U., Kölling, M., Bickert, T., 2007. Influence of the water content on X-ray fluorescence core-scanning measurements in soft marine sediments. *Geochem. Geophys. Geosyst.* 8, Q02004. <http://dx.doi.org/10.1029/2006GC001393>.
- Toyofuku, T., Duros, P., Fontanier, C., Mamo, B., Bichon, S., Buscail, R., Chabaud, G., Deflandre, B., Goubet, S., Grémare, A., Menniti, C., Fujii, M., Kawamura, K., Koho, K.A., Noda, A., Namegaya, Y., Oguri, K., Radakovitch, O., Murayama, M., de Noijer, L.J., Kurasawa, A., Ohkawara, N., Okutani, T., Sakaguchi, A., Jorissen, F., Reichert, G.-J., Kitazato, H., 2014. Unexpected biotic resilience on the Japanese seafloor caused by the 2011 Tōhoku-Oki tsunami. *Nat. Sci. Rep.* 4, 7517. <http://dx.doi.org/10.1038/srep07517>.
- Weltje, G.J., Tjallingii, R., 2008. Calibration of XRF core scanners for quantitative geochemical logging of sediment cores: theory and application. *Earth Planet. Sci. Lett.* 274, 423–438. <http://dx.doi.org/10.1016/j.epsl.2008.07.054>.
- Westerhold, T., 2003. The Middle Miocene Carbonate Crash: Relationship to Neogene Changes in Ocean Circulation and Global Climate. Universität Bremen.
- Zitellini, N., Mendes, L.A., Cordoba, D., Danobeitia, J., Nicolich, R., Pellis, G., Ribeiro, A., Sartori, R., Torelli, L., Bartolome, R., Bortoluzzi, G., Calafato, A., Carrilho, F., Casoni, L., Chierici, E., Corela, C., Correggiari, A., Vedova, B.D., Gracia, E., Jornet, P., Landuzzi, M., Ligi, M., Magagnoli, A., Marozzi, G., Matias, L., Penitenti, D., Rodriguez, P., Rovere, M., Terrinha, P., Vigliotti, L., Ruiz, A.Z., 2001. Source of 1755 Lisbon earthquake and tsunami investigated. *EOS Trans. Am. Geophys. Union* 82 (26), 285–296. <http://dx.doi.org/10.1029/EO082i026p00285-01>.